Arabian Journal of Chemistry (2022) **15**, 103517

King Saud University

Arabian Journal of Chemistry

www.ksu.edu.sa
www.sciencedirect.com

ORIGINAL ARTICLE

Green synthesis of platinum nanoparticles using *Atriplex halimus* leaves for potential antimicrobial, antioxidant, and catalytic applications

Abdelazeem S. Eltaweil [a,*], Manal Fawzy [b,c], Mohamed Hosny [b,*], Eman M. Abd El-Monaem [a], Tamer M. Tamer [d], Ahmed M. Omer [d]

[a] *Department of Chemistry, Faculty of Science, Alexandria University, Alexandria 21321, Egypt*
[b] *Green Technology Group, Environmental Sciences Department, Faculty of Science, Alexandria University, 21511 Alexandria, Egypt*
[c] *National Egyptian Biotechnology Experts Network, National Egyptian Academy for Scientific Research and Technology, Egypt*
[d] *Polymer Materials Research Department, Advanced Technology and New Materials Research Institute (ATNMRI), City of Scientific Research and Technological Applications (SRTA-City), New Borg El-Arab City, Alexandria P.O. Box 21934, Egypt*

Received 29 August 2021; accepted 19 October 2021
Available online 29 October 2021

KEYWORDS

Platinum;
Green synthesis;
Atriplex halimus;
Antibacterial;
Antioxidant;
Methylene blue

Abstract Herein, green platinum nanoparticles (PtNPs) were synthesized using an aqueous extract of *Atriplex halimus* leaves as a reductant. *Atriplex* platinum nanoparticles (At-PtNPs) were stable for up to three months. At-PtNPs were characterized by several techniques including UV–Visible spectroscopy, Fourier Transform Infrared (FT-IR) spectroscopy, X-ray diffraction (XRD), Energy Dispersive X-ray spectroscopy (EDX), EDX elemental mapping, High-resolution Transmission electron microscope (HRTEM), Selected Area Electron Diffraction (SAED), and X-ray Photoelectron Spectroscopy (XPS) and Zeta measurements. At-PtNPs were black-colored and mainly spherical with a plasmon peak at 295 nm with ultra-small particle size (1–3 nm) and high surface charge (−25.4 mV). At-PtNPs were verified as a superb catalyst as they were able to catalytically degrade MB dye. At-PtNPs exhibited a high antibacterial efficiency against gram-negative bacteria. At-PtNPs were proved as a highly efficient antioxidant agent. Thus, the attained results offer a promising route of the green synthesis of PtNPs using the aqueous extract of *Atriplex halimus*.

1. Introduction

In today's world, inorganic nanoparticles are a critical cornerstone that represents significant scientific and technological achievements (Abdelfatah, 2021; Mallikarjuna, 2017; Bathula, 2020; Eltaweil, 2020). Noble metal nanoparticles, including gold, silver, palladium, and platinum, have been proved to be applied in lots of different applications in mate-

* Corresponding authors.
E-mail addresses: abdelazeemeltaweil@alexu.edu.eg (A.S. Eltaweil), MohamedHosny@alexu.edu.eg (M. Hosny).
Peer review under responsibility of King Saud University.

Production and hosting by Elsevier

https://doi.org/10.1016/j.arabjc.2021.103517
1878-5352

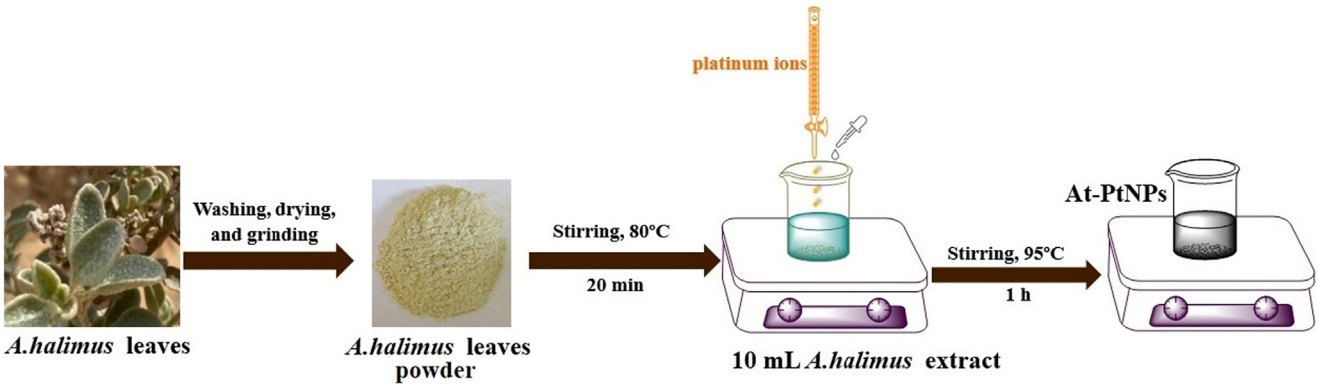

Fig. 1 Schematic representation for the green synthesis of PtNPs by *A. halimus* aqueous extract.

rial science, chemistry, and medicine (Jameel, 2020; Şahin, 2018; Mallikarjuna, 2019). Among these nanoparticles, platinum nanoparticles (PtNPs) have sparked special interest owing to their unique structural, optical, catalytic properties, high surface area, and good resistance to corrosion making them a potential candidate for catalysis and biomedical applications (Dong, 2021; Fan, 2021). PtNPs were reckoned to be efficient and can serve as drug carriers (Barua and Mitragotri, 2014; Al-Radadi, 2019). Also, PtNPs have a diversity of medicinal uses, including anti-cancer, anti-diabetic, antibacterial, and antifungal applications (Naseer, 2020).

Recently, green chemistry is urgently needed to synthesize environmentally sustainable products (Duan et al., 2015). Green synthesis of NPs has gained a lot of interest as the demand for non-toxic, safe, environmentally sustainable, and green procedures grow (Muthu and Priya, 2017; El-Borady et al., 2021). Plants are favored over other biological synthetic methods because they obviate the need for long times of bacterial and fungal culturing and preservation. Furthermore, extracellular plant extracts were proved to be more selective and powerful in regulating nanoparticle size, shape, and dispersity (Muthu and Priya, 2017). Therefore, employing plant extracts in the synthesis of nanoparticles advocates the principles of green chemistry including less hazardous chemical syntheses, safer solvents and auxiliaries, design for energy efficiency, and use of renewable feedstocks.

Plant sections such as roots, leaves, stems, and fruits have also been used to make NPs since their extract contains phytochemicals like flavonoids, tannins, and phenolic compounds that serve as both a reducing and stabilizing agent simultaneously (Rajeshkumar, 2016; Maisa'a and Awwad, 2021). Plants are employed in PtNPs synthesis because they are simpler, smoother, eco-friendly, durable, and cost-effective, and they produce more stable synthesized particles than other, more orthodox approaches (Aygun, 2020). *Nymphaea alba*; *Tragia involucrate*, and *Crocus sativus* are just some examples of plant extracts that were recently utilized in PtNPs synthesis.

A substantial environmental concern comes from the textile industry's release of harmful dyes, especially into aquatic areas (El-Monaem, 2021; Eltaweil, 2021; Chandrasekaran et al., 2020; Arul et al., 2020; Arul, 2021; Eltaweil, 2021). Methylene blue (MB), which is a common harmful dye, inhibits sunlight from reaching a water body so it has a long-term negative impact on the aquatic ecosystem (Eltaweil, 2020; Eltaweil, 2020). Therefore, this deleterious dye was chosen to test the catalytic degradation potency of the phytosynthesized At-PtNPs in this work.

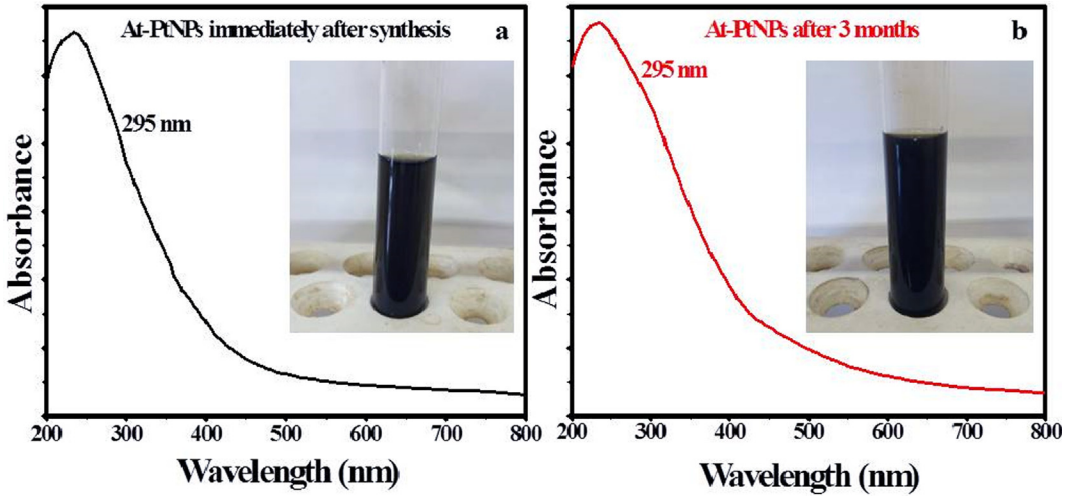

Fig. 2 UV–Vis spectrum and images (inset) of At-PtNPs **(a)** Immediately after synthesis and **(b)** After 3 months.

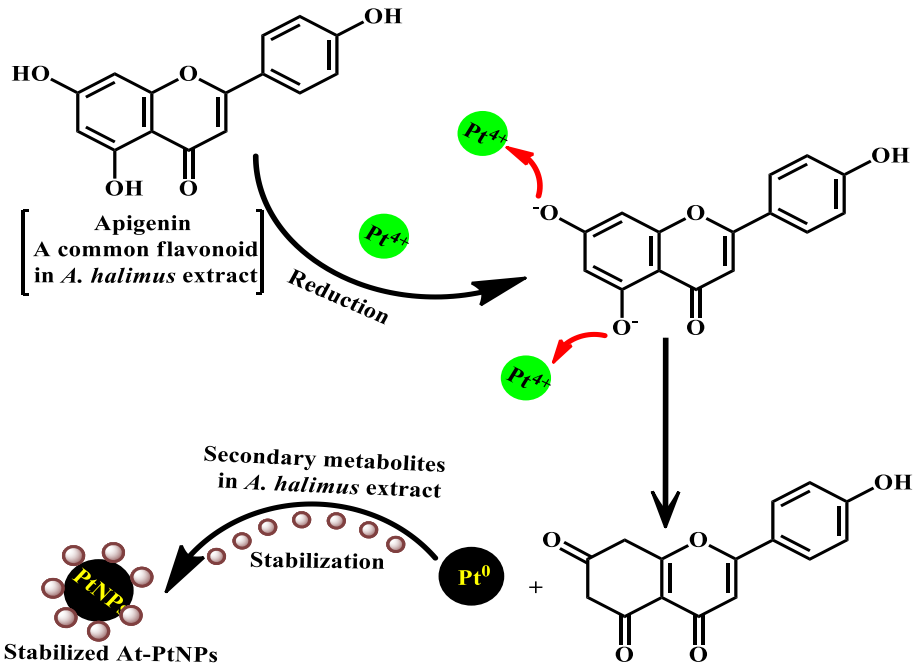

Scheme 1 A plausible mechanism for the reduction of Pt^{4+} by polyphenols in *A.halimus* aqueous extract.

Generally, bacterial pathogens are suspected of causing a wide range of life-threatening illnesses in people and animals (Selvi, 2020; Omer, 2021). Bacterial strains whether gram-negative or gram-positive bacteria such as *Escherichia coli* and *Staphylococcus aureus* that are commonly existing in the environment, food, and the intestines of people and animals (Iyer, 2018), can result in severe dermal infections, problems with urinary and respiratory tract systems, and intravenous catheters especially in immune-compromised patients (Carezzano, 2017). Various antibiotics were employed in the treatment of these pathogenic bacteria yet continuous application or consumption of these antibiotics resulted in the development of drug-resistant bacteria (Allen, 2010). Thus, novel materials such as PtNPs have to be synthesized and employed in such an onerous task. Additionally, the antifungal activities of biogenic synthesized PtNPs against various fungal species were previously reported (Wang and Lippard, 2005).

Methods for estimating the efficacy of nanoparticles such as antioxidants are becoming more common. In addition, the use of the stable free radical 1,1-diphenyl-2-picrylhydrazyl (DPPH) is one such process that is currently common for the assessment of nanoparticles as antioxidants (Chen, 2021).

Herein, the aqueous extract of *A. halimus* leaves was utilized for the first time in PtNPs synthesis and stabilization as a green and efficient route for the synthesis of PtNPs with excellent catalytic and biological activities as well as very high stability. Therefore, the aim of the current work is twofold, firstly to investigate the potentiality of *A. halimus* leaves aqueous extract in the synthesis of highly stable PtNPs and secondly to test the applicability of At-PtNPs in medical applications including antibacterial and antioxidant test and also in the catalytic degradation of MB.

2. Materials and methods

2.1. Chemicals and reagents

All reagents used in this study were of analytical grade and used without purification including hexachloroplatinic acid

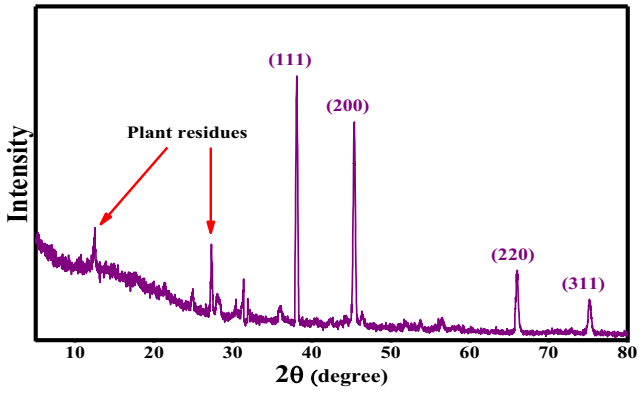

Fig. 3 XRD pattern of At-PtNPs.

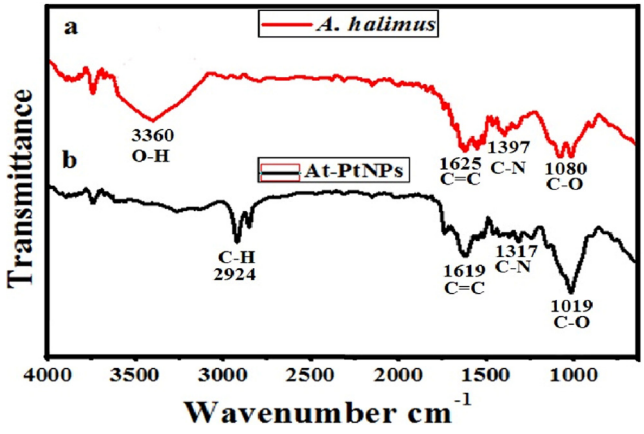

Fig. 4 FT-IR spectra of *A. halimus* **(a)** and At-PtNPs **(b)**.

($H_2PtCl_6{\cdot}6H_2O$), sodium hydroxide (NaOH), sodium borohydride ($NaBH_4$), and methylene blue (MB) were purchased from Merck, USA.

2.2. Collection of plant specimens and preparation of extracts

Representative samples of *A. halimus* leaves were collected from their natural habitats on the Mediterranean coastal land of Egypt and the Nile Delta. Leaves were rinsed with deionized water (D.W.) numerous times to remove any impurities and debris. Then leaves were shredded and allowed to dry in the open air followed by overnight drying at 60 °C till reaching constant weight. Afterward, dry leaves were ground in a stainless steel mixer to have a fine powder. Five grams from the resultant powder were mixed with 100 mL of D.W, then the mixture was heated at 80 °C and stirred at 500 rpm using a magnetic stirrer for approximately 20 min. Eventually, the hot solution was filtered and the filtrate was stored in a glass beaker at 4.0 °C for further use.

2.3. Green synthesis of PtNPs

Briefly, 10 mL of *A. halimus* leaves extract was added to 1 mL of platinum chloride solution ($H_2PtCl_6{\cdot}6H_2O$) with a molarity of 0.0019 M. Afterwards, to achieve fast synthesis process, the pH of the mixture solution was adjusted at 9.6 (based on preliminary experiments) using NaOH (0.1 M) then the mixture solution was subjected to stirring and heating at 95 °C for almost one hour till a color change was observed from dark yellow to black. The purification step was carried out by centrifugation of *A. halimus*-PtNPs (At-PtNPs) colloidal solution then collecting the precipitated pellets and washing them using repeatedly with D.W. Then the formed At-PtNPs solution was preserved at 4.0 °C.

2.4. Characterization techniques

The UV–Visible spectroscopy measurements (200–800 nm) using a double-beam spectrophotometer (T70/T80 series UV/Vis Spectrophotometer, PG instruments Ltd, UK) to ensure the green reduction of the Pt^{4+} into PtNPs. HRTEM measurements were done on a JOEL, JEM-2100F, Japan, accelerating voltage of 200 kV FT-IR spectra were conducted using a JASCO spectrometer to assess the possible involvement of functional groups in *A. halimus* extract that were responsible for the reduction and stabilization process. Zeta potential and hydrodynamic size of fabricated At-PtNPs was examined in a zeta potential analyzer (Zetasizer Nano ZS Malvern) to determine the surface charge of At-PtNPs. The XRD measurements of powdered At-PtNPs were done on an X-ray diffractometer (X'PERT PRO. Netherland) operated at a voltage of (45KV) and current of (40 mA) with CuKa1 radiation ($\lambda = 1.54056A^{o}$) in the 2θ range from 20° to 80° to make sure of the crystalline nature of At-PtNPs. The crystallite size was calculated from the width of the XRD peaks using the Scherrer formula as given by:

$$(D) = \frac{0.9\lambda}{\beta \cos\theta}$$

Where D is average crystallite size, β indicates the line broadening the value of the full width at half maximum (FWHM) of a peak, λ is the wavelength of irradiated X-rays, and θ is the maximum peak position value. Energy-dispersive X-ray spectroscopy (EDX), performed using JEOL model JSM-IT100 to investigate the elemental composition of At-PtNPs. XPS was collected on K-ALPHA (Thermo Fisher Scientific, USA) with monochromatic X-ray Al K-alpha radiation −10 to 1350 eV spot size 400 micro m at pressure 10^{-9} mbar with full-spectrum and narrow-spectrum 50 eV to confirm the reduction of Pt^{4+} into Pt^{0}.

2.5. Catalytic degradation of MB

100 μL of freshly prepared aqueous $NaBH_4$ solution (0.058 M) were added to 10 mL of MB (20–100 ppm). Subsequently, 100 μL of At-PtNPs with a concentration of 50 μg/mL were added to the mixture at 25° C with continuous stirring. The reaction was monitored by recording the time-dependent UV–Vis absorption spectra of these mixtures at 664 nm. Control experiments were conducted using the same experimental conditions yet without At-PtNPs and/or $NaBH_4$. The degradation efficacy was measured by the following equation:

$$\text{Removal}\% = \frac{A_0 - A}{A_0} \times 100 \quad (1)$$

Where (A_0) represents the initial absorbance of MB at time 0, while (A) refers to the absorbance of MB at time t.

2.6. Antimicrobial test

Inoculum preparation: The stock culture of reference strain (in glycerol broth) was subcultured onto tryptic soy agar plates. The tested samples are *Escherichia coli* (ATCC 8739), *Klebsiella pneumonia* (ATCC 1388), *Bacillus subtilis* (ATCC 6633), and *Staphyllococcus aureus* (MRSA)(ATCC 25923). Turbidity of the suspended colonies was compared with the 0.5 McFarland turbidity standard equivalent to $2x10^{8}$ CFU/mL.

Preparation of seeded agar: Muller Hinton agar is weighed and dissolved in distilled water then sterilized by autoclaving after being divided into 25 mL portions into 6 separate flasks. Flasks were shaken and poured onto sterile petri dishes and left to solidify.

Placing of tested materials (At-PtNPs): At-PtNPs were placed directly in wells after sterilization by filtration; the plates were put in the refrigerator overnight to allow diffusion of At-PtNPs material.

Incubation: Plates were incubated at 35 ± 2 °C for 24 h.

Reading results: All measurements were made with the unaided eye while viewing the back of the Petri dish a few inches above a non-reflecting background and illuminated with reflected light.

2.7. Antioxidant activity of PtNPs (DPPH assay)

The free radical scavenging activity was examined via DPPH (2, 2-diphenyl-1-picrylhydrazyl) assay to determine the antioxidant efficiency of At-PtNPs samples. The assay was conducted in triplicates. In the process, 1 mL of each PtNPs sample was mixed with 1 mL of DPPH (0.2 mM) along with control DPPH which does not contain any nanoparticles. This mixture was blended for 3 min in dark conditions at ambient tempera-

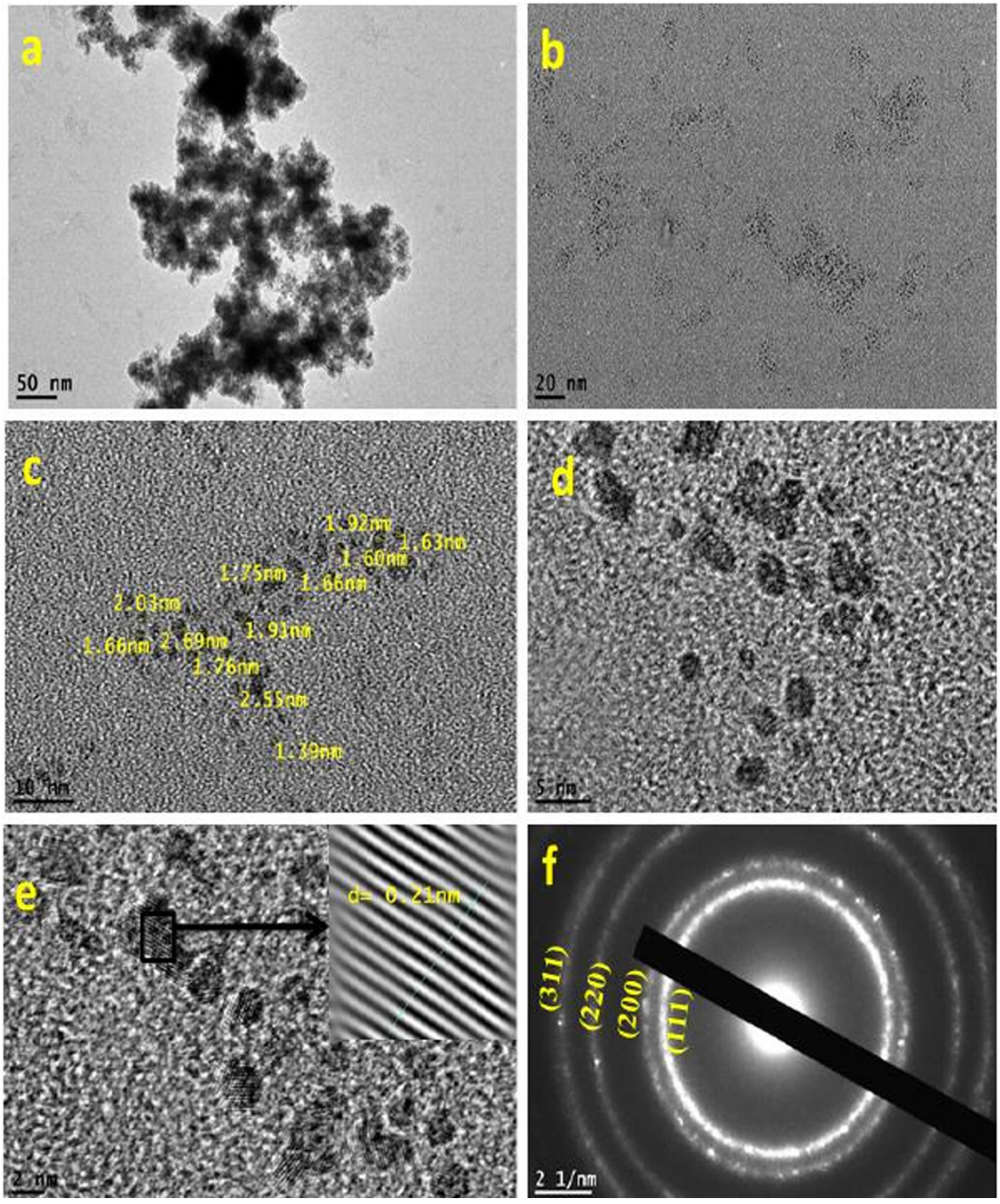

Fig. 5 **(a-e)** HRTEM images of At-PtNPs **(f)** SAED image of At-PtNPs **(g)** Size distribution of At-PtNPs.

ture. Then, after 20 min the concentration of radical is examined by the reduction in absorbance percentage of the mixture at 517 nm wavelength. The control was set up as over. Change in absorbance was estimated at 517 nm. Vitamin C (ascorbic acid) was used as a reference (positive control). The activity was measured by the following equation (El-Borady, 2020).

$$\text{Radicalscavengingactivity} = \frac{(Controlabsorbance - sampleabsorbance) \times 100}{controlabsorbance} \quad (2)$$

Where control absorbance is the absorbance in the absence of antioxidants and sample absorbance is the absorbance in the presence of antioxidants (At-PtNPs or Vitamin C) at 517 nm.

2.8. Statistical analysis

All experiments were conducted in triplicate (n = 3), while the gained data were presented as a mean value corrected by the standard deviation (±SD).

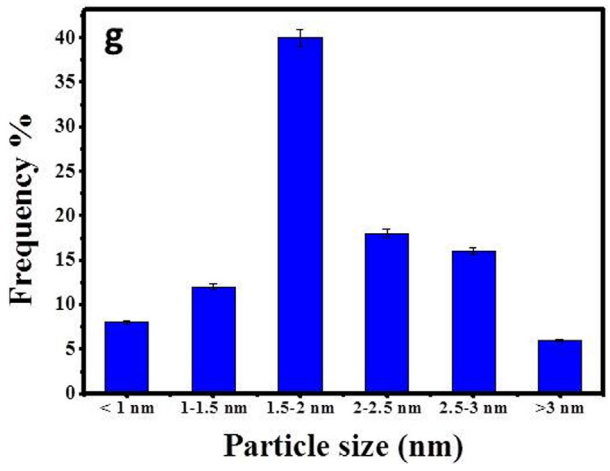

Fig. 5 (*continued*)

3. Results and discussion

3.1. Characterization of At-PtNPs

A.halimus aqueous extract was previously confirmed to contain a diversity of phytoconstituents, including flavonoids, glycosides, and alkaloids (Benhammou et al., 2009; Walker, 2014). As a result, Fig. 1 was used to represent a simplified mechanism for the phytosynthesis of At-PtNPs using *A.halimus* aqueous extract. Consequently, there was no need for any chemicals. These phytoconstituents are postulated to play a dual role as a reducing and stabilizing agent at the same time since they were proven to be capable of donating electrons or hydrogen atoms to platinum ions to get these ions reduced (Brewer, 2011). Firstly, *A.halimus* extract reduced platinum ions into a metallic or zero-valent form of platinum (PtNPs). Secondly, they contributed to the stability of the resultant At-PtNPs as they remained stable for more than three months as displayed in Fig. 2**a and b**. Thus, confirming the great potentiality of *A.halimus* aqueous extract in the phytosynthesis of several metallic and non-metallic nanoparticles in the near future and denoting its cost-effectiveness. Especially, *A.halimus* strains that are affected by environmental pressures including droughts and high levels of salinity as it was proven that the concentration of the phytoconstituents increases in most living plant species when the severity of these environmental pressures increases (Oh et al., 2009).

Moreover, the plausible mechanism for the reduction of Pt^{4+} by polyphenols in *A.halimus* aqueous extract is elucidated in Scheme 1.

3.2. UV–Visible spectroscopy

The excitation produced by a source of light at a certain wavelength has a distinct peak at that wavelength known as surface plasmonic resonance which is determined by UV–visible spectroscopy (Zada, 2018). Most of the metallic nanoparticles have unique surface plasmon resonance (SPR) bands (Noruzi et al., 2012). Moreover, the NPs shape and size usually define the form and location of the SPR peak. In the current study, a black-colored colloidal solution (**Inset** Fig. 2**a**) and an SPR peak that appeared at 295 nm as shown in Fig. 2**a** which is characteristic to PtNPs confirmed the successful phytosynthesis of At-PtNPs using the aqueous extract of *A. halimus*. Furthermore, At-PtNPs were stable for up to three months as indicated by the unaffected black color (**Inset** Fig. 2**b**) and UV–Vis surface plasmon resonance (Fig. 2**b**). Concomitantly with the current study, other researchers reported similar results for the characteristic peak of green synthesized PtNPs (Al-Radadi, 2019; Thirumurugan, 2016).

3.3. XRD analysis

The face-centered cubic crystalline structure of At-PtNPs was confirmed by the XRD pattern. Distinct diffraction peaks of PtNPs at 38.1°, 44.6°, 64.7°, and 78.3° corresponding to (1 1 1), (2 0 0), (2 2 0), and (3 1 1) planes were observed (Fig. 3). Furthermore, the green synthesized At-PtNPs' preferred growth orientation was the (1 1 1) plane. The obtained results matched the stated requirements for crystalline platinum; JCPDS file no. 04–0802. The Scherrer formula was used to determine the average crystallite size of At-PtNPs, which was found to be about 1.5 nm, which was close to the size range (1–2 nm) observed by HRTEM spectroscopy. The undefined sharp peaks are attributed to the plant residues (Hosny, 2021). In addition, the smaller crystallite size reported in this study suggesting the higher proficiency for the synthesized At-PtNPs.

3.4. FT-IR analysis

FTIR spectrum of *A. halimus* showed several peaks at different wavenumbers including O-H group at 3360 cm^{-1}, C = C group at 1625 cm^{-1}, C–N group at 1397 cm^{-1}, and C-O stretching group at 1080 cm^{-1} (Fig. 4**a**). However, in the spectrum of At-PtNPs (Fig. 4**b**), some of these peaks appeared but at a lower wavenumber including the C = C group at 1619 cm^{-1}, C–N group at 1317 cm^{-1}, and C-O group at 1019 cm^{-1}. Also, the O-H group of *A. halimus* disappeared confirming the active role of O-H functional group-containing phytoconstituents in the reduction and stabilization

Table 1 Comparison between the physical properties of At-PtNPs and other green synthesized PtNPs.

Plant	Size (nm)	Shape	Zeta potential (mV)	Ref.
Maytenus royleanus	5	Spherical	−41	(Ullah, 2017)
Taraxacum laevigatum	2–7	Spherical	−29	(Tahir, 2017)
Garcinia mangostana L.	~2	Spherical	−13	(Nishanthi et al., 2019)
Prosopis farcta	10–40	Spherical	−15.6	(Jameel et al., 2020)
Atriplex halimus	1–3	Spherical	−25.4	Current study

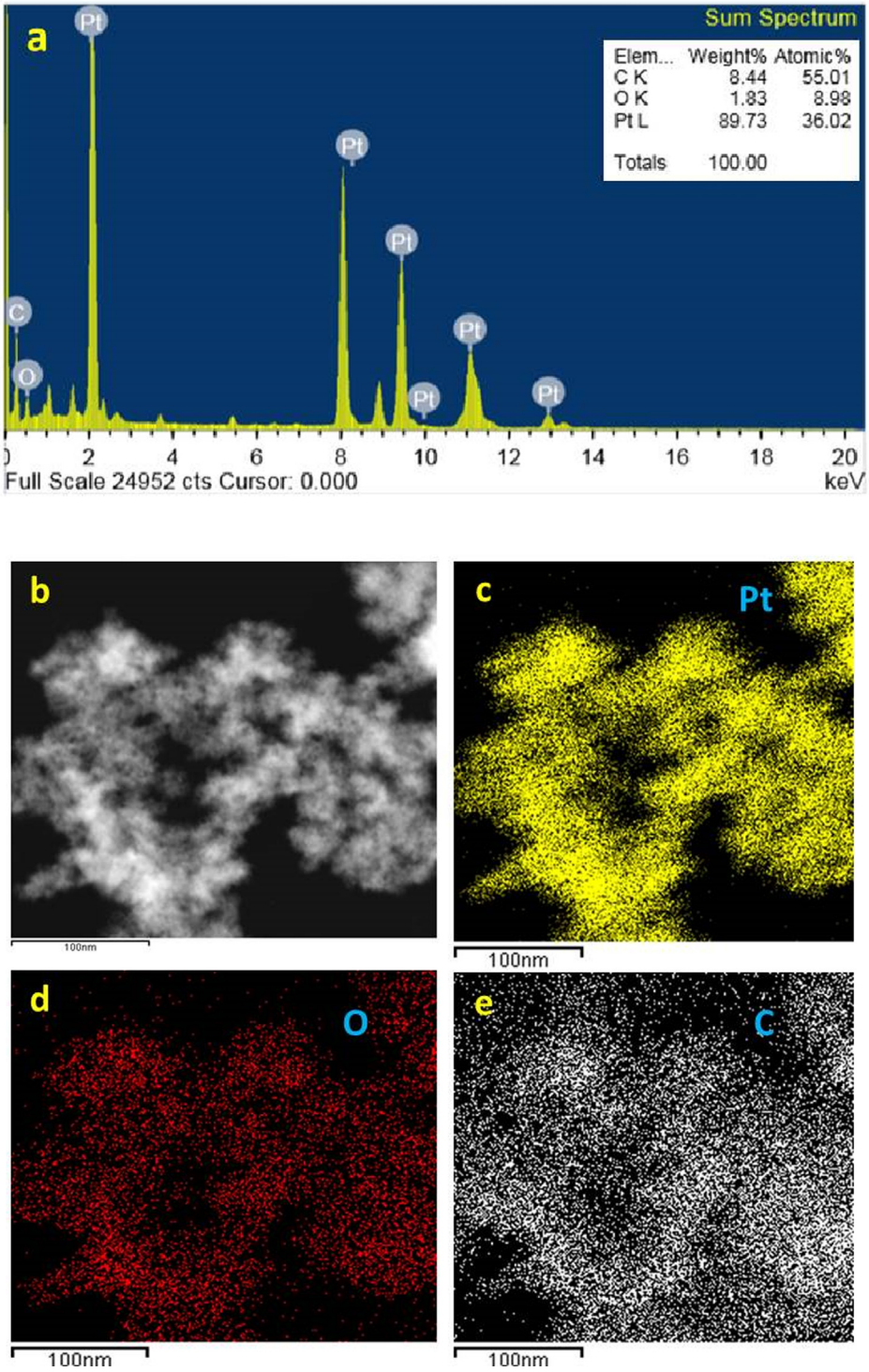

Fig. 6 **(a)** EDX of At-PtNPs **(b-e)** elemental mapping images of At-PtNPs.

of At-PtNPs. In addition, a new C–H stretch appeared at 2920 cm^{-1} and 2850 cm^{-1}. Consequently, it was concluded that phytoconstituents of *A. halimus* extract including glycosides, terpenoids, flavonoids, and alkaloids (Rahman, 2011) were responsible for the reduction and capping of At-PtNPs. The current results are concomitant with other previously published works that were concerned with the green synthesis of PtNPs (Thirumurugan, 2016; Yang, 2017). The obtained results indicated that the dielectric constant of the medium may have been changed because of the involvement of a variety of different phytochemicals from *A. halimus* extract such as glycosides, flavonoids, phenolic acids, and alkaloids as capping

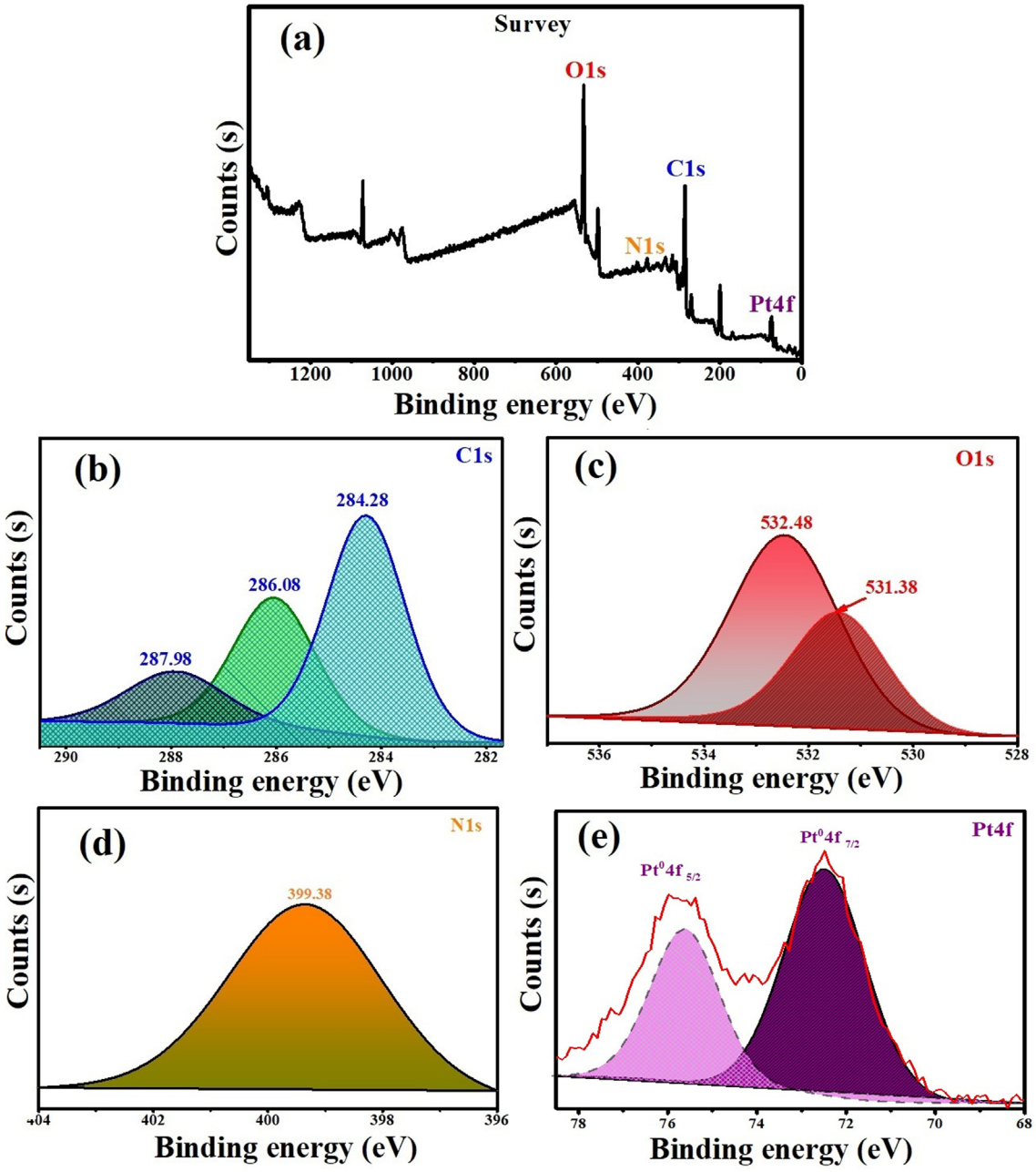

Fig. 7 XPS spectrum of At-PtNPs (a) survey (b) C1s (c) O1s (d) N1s (e) Pt4f.

agents which are supposed to cause the deviation or the shift of the peak positions in the At-PtNPs spectrum as previously elaborated (Mahmoud, 2012; Pandey and Mishra, 2014).

3.5. High resolution transmission electron microscopy (HRTEM)

Providing essential information of nanoparticles such as shape and size is usually achieved by using High Resolution Transmission electron microscopy (HRTEM) (Hosny, 2021). It was found that the average particle size of At-PtNPs approximately ranged between 1 and 3 nm as shown in Fig. 5 **(a-e)**, similar to other previous works (Jameel, 2020; Tahir, 2017), which is a very small particle size that could result in outstanding efficiency when these nanoparticles used in various applications. When the hydrodynamic size was measured *via* zetasizer as previously done by (Cui, 2021), it was found to be 9.4 nm. It has to be noticed that the hydrodynamic size is larger than the HRTEM particle size as it includes the size of biomolecules that are capping the nanoparticles (Dong, 2021; Ullah, 2017). The predominantly observed shape was spherical. The crystalline structure of At-PtNPs was confirmed by utilizing the Selected Area Electron Diffraction (SAED) technique demonstrated in Fig. 5**f**. SAED results were concomitant with the results obtained from XRD analysis indicating the (1 1 1), (2 0 0), (2 2 0), and (3 1 1) planes of crystalline At-PtNPs. In

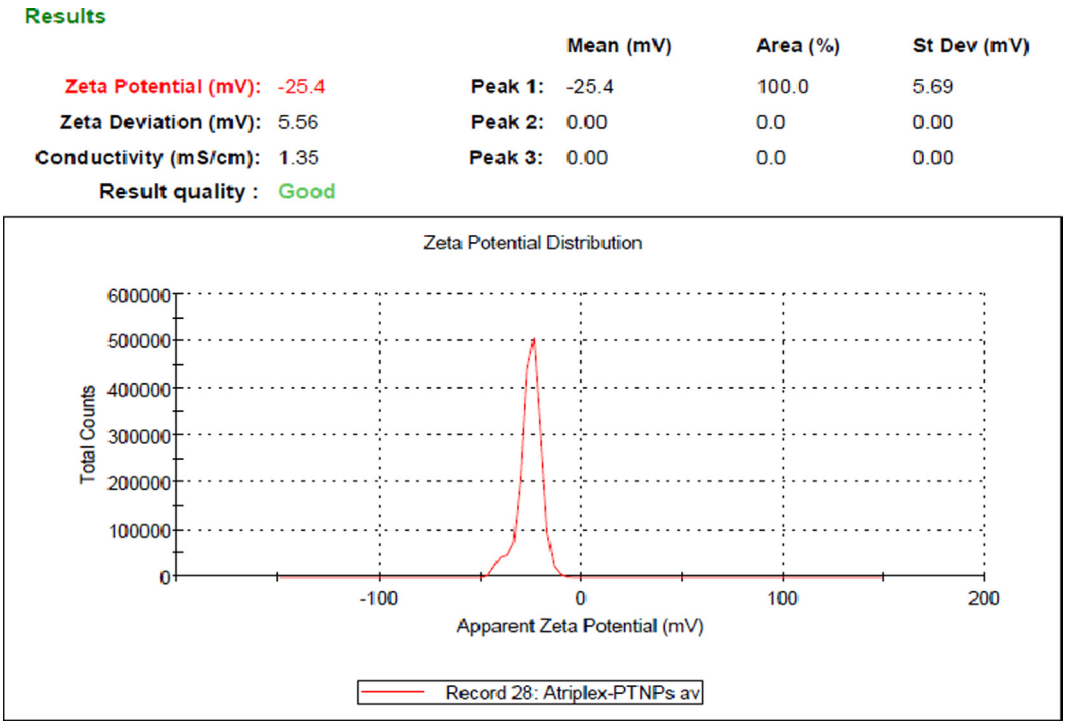

Fig. 8 Zeta potential of At-PtNPs.

addition, crystalline At-PtNPs consisted of several crystalline lattices with well-defined inter-planer spacing d = 0.21 nm that is shown in **(inset)** Fig. 5**e**. Furthermore, a histogram size distribution of At-PtNPs that is presented in Fig. 5**g** indicated that approximately 40 % of these particles lie in the size range of 1.5–2 nm. The obtained results were in line with other previous studies (Jameel et al., 2020; Nishanthi et al., 2019). Furthermore, a comparison between the physical properties of At-PtNPs and other green synthesized PtNPs is presented in Table 1.

3.6. EDX analysis and mapping

Energy-dispersive X-ray spectroscopy (EDX) was used to confirm the phytoreduction of $H_2PtCl_6{\cdot}6H_2O$ into At-PtNPs. This was confirmed by strong signals of elemental platinum at energy levels of 2.2, 8.2, 9.5, 10, 11.2, and 13 keV in At-PtNPs as shown in Fig. 6**a** which are concomitant with the results of other workers (Konishi, 2007). It has to be pointed that the percentage of elemental platinum in At-PtNPs was approximately 90 % indicating the outstanding efficiency of *A. halimus* leaves extract in the phytosynthesis of At-PtNPs. Carbon and oxygen were derived from *A. halimus* extract. Also, carbon was derived from the carbon-coated copper grid. In the current analysis, the atoms on the At-PtNPs were excited by a specific wavelength electron beam. These, in turn, emit X-rays at an energy level that is element-specific as previously indicated (Bharati and M., C. Byram, and V.R. Soma, , 2018). As revealed in Fig. 6**c**, the yellow EDX mapping revealed that the nanoparticles presented in Fig. 6**b** are composed of platinum because the yellow color is centered over At-PtNPs. Similar results were obtained by Yang et al. (Yang, 2018). Furthermore, the red EDX mapping, as illustrated in Fig. 6**d**, indicated that the oxygen was equally distributed all over the map. Thus, confirming that the At-PtNPs are of zero-valent state of platinum (Pt_0), not platinum oxide (PtO_2) nanoparticles. Moreover, the white color in Fig. 6**e** represented the carbon that was equally distributed all over the map. Therefore, the obtained results designated that the oxygen and carbon were resulting from the phytoconstituents of *A. halimus* extract. In other words, they were of plant origin.

3.7. XPS analysis

In the current investigation, XPS analysis was used to determine the oxidation state of At-PtNPs as it was previously utilized (Aygun, 2020; Zou, 2018). Pt, C, O, and N were found to be the most prevalent elements in our findings as shown in the survey in Fig. 7**a**. High resolution spectrum of C1s (Fig. 7**b)** showed three main peaks with binding energies of 284.28, 286.08, and 287.98 eV resulting from hydrocarbon chains, α-carbon, and single bond COOH groups present in the *A. halimus*'s phytoconstituents as it was elaborated by Syed and Ahmad (Syed and Ahmad, 2012). The peaks in Fig. 7**c** correspond to chemically distinct O1s and with binding energies at 531.38 eV and 532.48 eV that are attributed to the carbonyl group and molecular water (Hussain, 2019). While Fig. 7**d** demonstrated a peak at 399.78 eV which is related to N1s core levels. The obtained high-resolution spectrum of Pt4f (Fig. 7**e)** was characteristic for metallic Pt with $Pt^0 4f_{7/2}$ and $Pt^0 4f_{5/2}$ at binding energies of 72.48 and 75.58 eV, respectively. The obtained results were concomitant with other published ones (Celebioglu, 2017; Benaissi, 2010). As a result, At-PtNPs were concluded to be in the metallic Pt_0 form (only the zero-valent state is produced), rather than Pt^{2+} or Pt^{4+}. The obtained

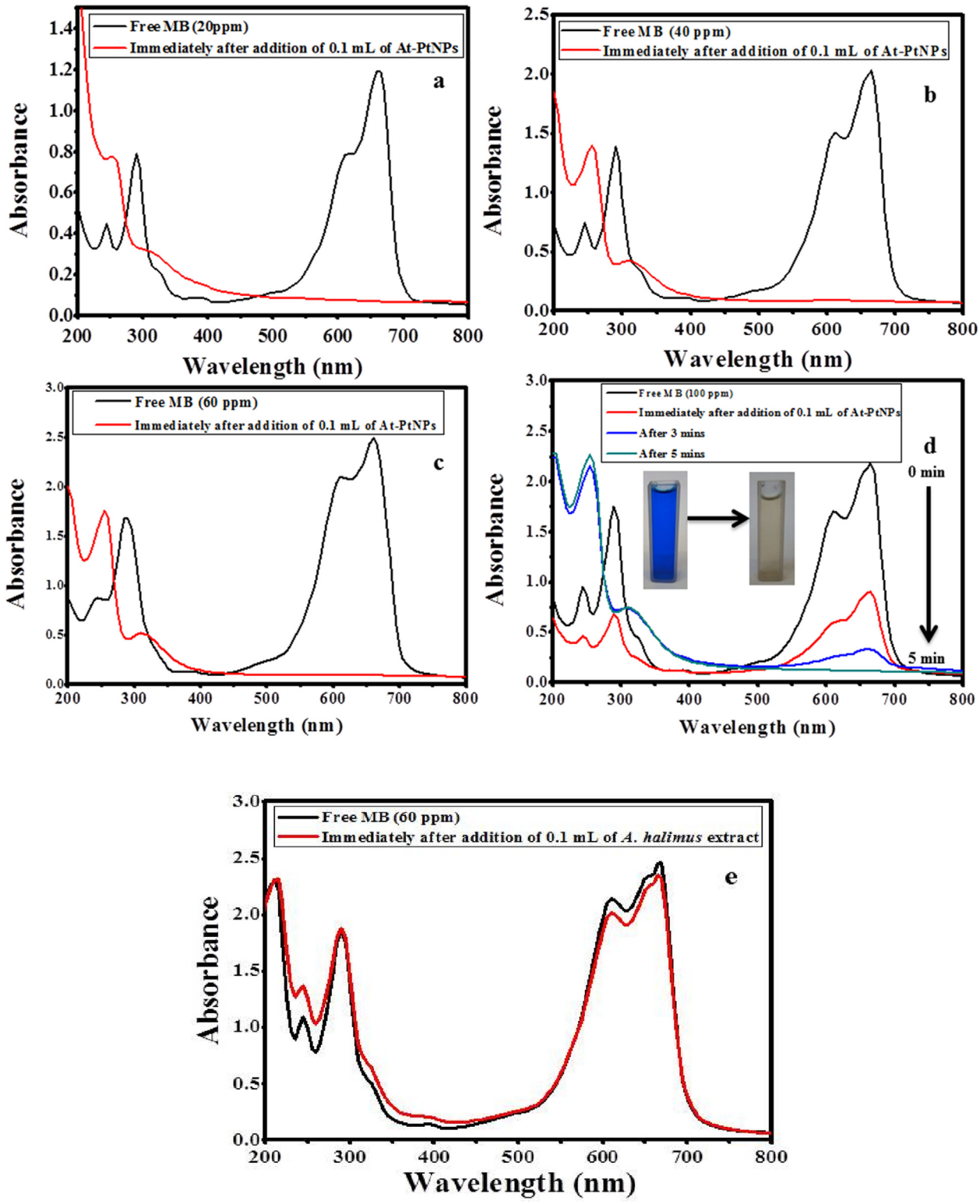

Fig. 9 Catalytic degradation of MB **(a)** 20 ppm **(b)** 40 ppm **(c)** 60 ppm **(d)** 100 ppm using100 µL of At-PtNPs **(e)** Catalytic degradation of MB (60 ppm) using100 µL of *A. halimus* extract.

result may be explained by the straightforward reduction of an oxidized platinum species to its zero-valent form (the stable state of Pt) by the action of phytoconstituents found in *A. halimus* extract.

3.8. Zeta potential

The stability and surface charge of green synthesized At-PtNPs were investigated using a zeta analyzer. This approach is com-

Table 2 A Comparison between the catalytic degradation efficiency of At-PtNPs and other nanoparticles that were reported in other studies against MB.

Catalyst	MB concentration (ppm)	Degradation efficiency (%)	Time (min)	Ref.
AuNPs	–	100	12	(Bogireddy et al., 2015)
AuNPs	50	100	10	(Hosny, 2021)
AuNPs	320	100	9	(Ganapuram, 2015)
AgNPs	16	100	30	(Edison, 2016)
AgNPs	320	100	20	(Bonnia, 2016)
PdNPs	240	100	2	(Kora and Rastogi, 2016)
PdNPs	25	100	5	(Subhan, 2020)
PdNPs	3	70	75	(Anand, 2016)
PtNPs	10	100	15	(Jameel, 2020)
At-PtNPs	25–75	100	Immediate	**This study**
At-PtNPs	100	100	5	**This study**

monly utilized to measure nanoparticles dispersion stability (Tahir, 2017). At-PtNPs had a zeta potential value of − 25.4 mV (Fig. 8), confirming the high stability of At-PtNPs. As the zeta potential value becomes more negative, nanoparticles become more stable (Shah, 2014). At-PtNPs have a negative zeta potential, denoting that they are capped with negatively charged phytoconstituents that cause repulsion (dispersion) among them and increase their stability. The obtained results in the current study were lower than (Ullah, 2017) who mentioned that the zeta potential of PtNPs was − 41 mV and higher than that of (Dong, 2021) who reported a zeta value of − 7.33 mV.

3.9. Applications of green synthesized At-PtNPs

3.9.1. Catalytic degradation of MB

In the current study, the catalytic degradation of different concentrations (20, 40, 60 and, 100 ppm) MB was conducted using 100 µL of At-PtNPs in the presence of 100 µL of 0.058 M $NaBH_4$. The obtained results indicated that the characteristic blue color of the three concentrations (20, 40, and 60 ppm) of MB instantly disappeared after the addition of At-PtNPs to confirm the complete degradation of MB as shown in Fig. 9 **(a-c)**. However, in the case of the highest concentration (100 ppm), it took approximately five min for complete MB degradation and color removal as shown in Fig. 9**d** and **inset of** Fig. 9**d**, respectively. When control experiments were carried out either without $NaBH_4$ or At-PtNPs there was no color change observed. Moreover, when the catalytic effect of *A. halimus* extract was tested, it was figured out that the removal efficiency was only 4% as shown in Fig. 9**e** indicating the essential role of At-PtNPs in the catalytic degradation of MB. It has to be noticed that the obtained results in this study were reckoned to be superior to those reported by Dobrucka (Dobrucka, 2019) who reached a catalytic efficiency of approximately 37.5 % for MB solution with a concentration of just 40 ppm using PtNPs phytosynthesized by the extract of *Fumariae herba* after 15 min. As well as, our results are far away better than the results attained by Jameel et al. (Jameel, 2020) who achieved complete degradation of MB with a concentration of only 10 ppm in 15 min using sonochemical synthesized PtNPs. Therefore, it was concluded that the green synthesized At-PtNPs in the current study unequivocally have a better performance than other phyto or chemically synthesized PtNPs, which could be accredited to the phytoconstituents of *A. halimus* extract that resulted in the formation of highly stable and efficient PtNPs. Therefore, it is considered to be a highly potent and prominent catalyst that could be harnessed in the catalytic degradation of other toxic dyes from wastewater. In addition, a detailed comparison between At-PtNPs and other nanocatalysts including different variables such as the dye concentration, the degradation efficiency, and time is provided in Table 2. From Table 2, it can be concluded that the synthesized At-PtNPs are highly efficient for the catalytic degradation of MB.

Five cycles of At-PtNPs utilization in the removal of MB with a concentration of 60 ppm were carried out to test their reusability. The obtained results indicated that the removal efficiency remained 100% after three cycles of regeneration (Fig. 10**a, b, c**). However, the efficiency started to diminish slightly to 93% in the fourth cycle (Fig. 10**d**) and eventually it reached 91.1% (Fig. 10**e**) after five cycles of reuse confirming the great potentiality of At-PtNPs as a catalyst as shown in Fig. 10**f**.

A suggested mechanism that is concomitant with previous ones using other types of nanoparticles including AgNPs and AuNPs (Atta, 2020) for the catalytic degradation of MB into leuco MB is illustrated in Fig. 11**.** The reduction process occurs as both MB and BH_4^- ions are adsorbed on the surface of At-PtNPs and an electron relaying from the BH_4^- ions to the MB molecules resulting in the catalytic degradation of MB into leuco (El-Subruiti et al., 2019; Sallam et al., 2018). It has to be noticed that the degradation of dimethylamino groups in MB molecule by strong catalysts such as At-PtNPs facilitates the removal of MB. In addition, when Liu et al. (Liu, 2014) investigated the final products of MB molecules after its catalytic degradation using Ion Chromatography (IC), they observed that MB molecules were totally degraded into inorganic compounds such as NH_4^+, S^{2-}, SO_4^{2-}, NO_3^-, CO_2, and H_2O.

3.9.2. Antimicrobial study of At-PtNPs

The efficacy of green produced At-PtNPs at a concentration of 1 $mg.L^{-1}$ as an antibacterial agent against gram-negative and

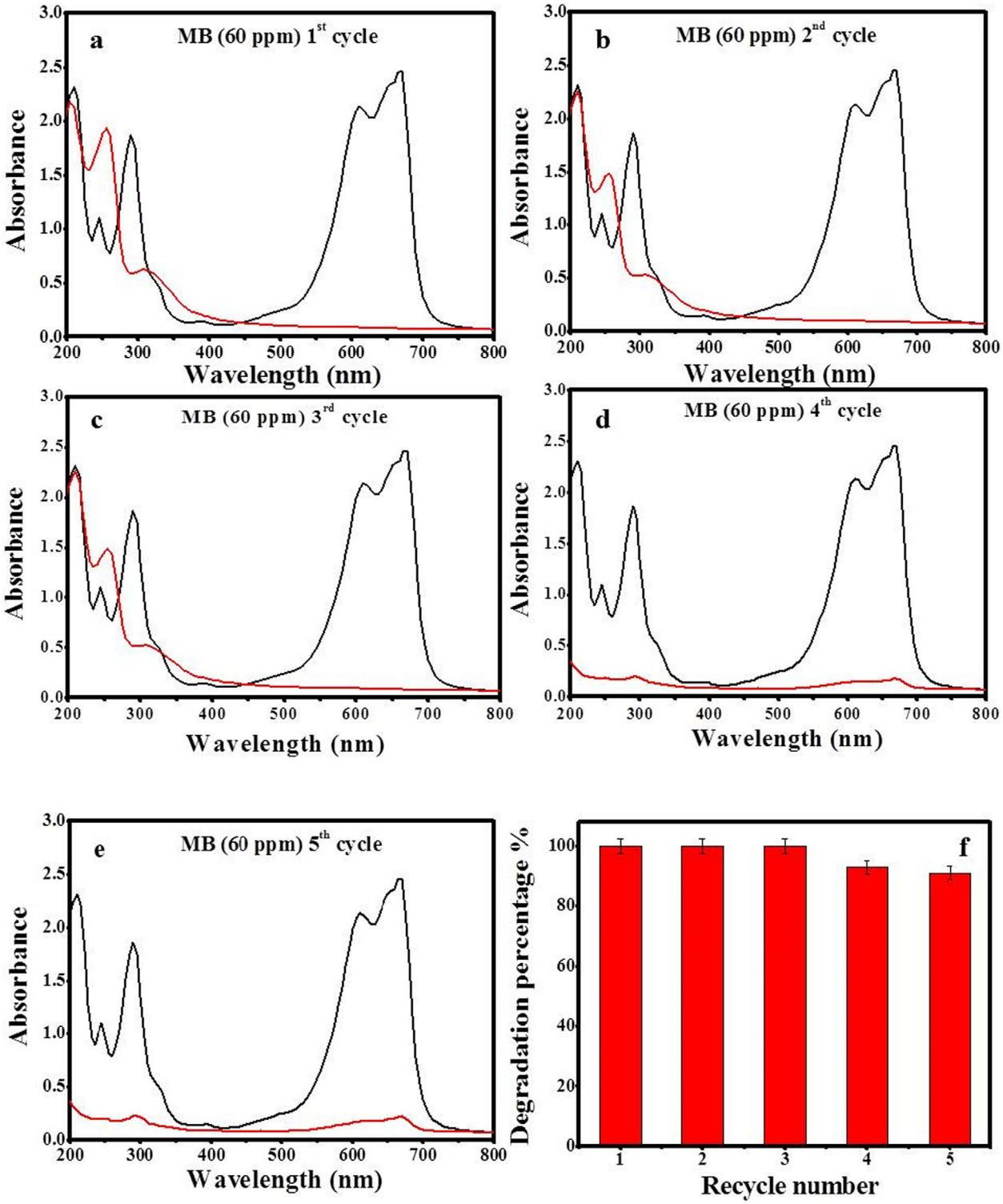

Fig. 10 Recycling of At-PtNPs against MB (60 ppm) **(a)** 1st cycle **(b)** 2nd cycle **(c)** 3rd cycle **(d)** 4th cycle **(e)** 5th cycle **(f)** degradation percentage with recycling number.

gram-positive bacteria was determined using the zone of inhibition as shown in Fig. 12. The bacterial strains which were used in the current study are *Escherichia coli*, and *Klebsiella pneumonia* (gram-negative bacteria), and also gram-positive bacteria such as *Bacillus subtilis* and *Staphyllococcus aureus* (Mrsa). Our results showed that the inhibition zone was 17 mm for *Klebsiella pneumonia* and no growth was detected at all in the case of *Escherichia coli* indicating that At-PtNPs were highly efficient against *Escherichia coli* as it prevented the growth of the bacteria. However, At-PtNPs did not show

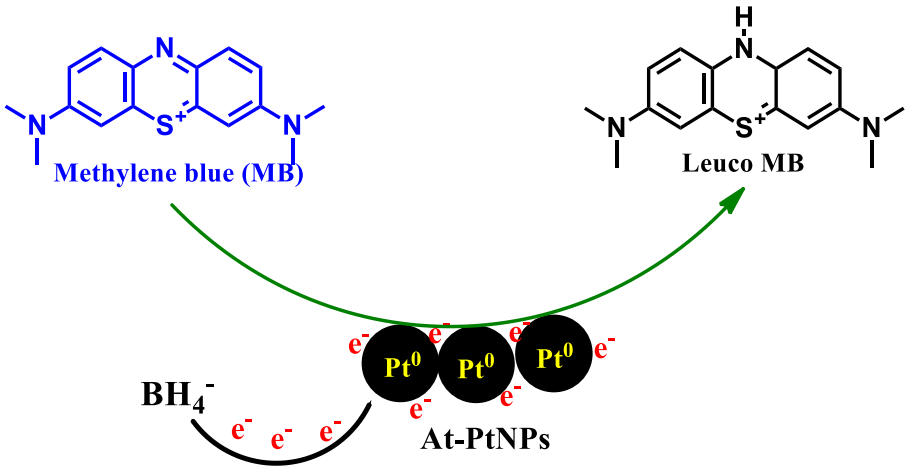

Fig. 11 A proposed mechanism for the catalytic degradation of methylene blue (MB) into leuco MB onto At-PtNPs.

any activity against gram-positive bacteria. As a result of the current findings, At-PtNPs may have antibacterial characteristics by changing the shape of the cell membrane and inhibiting normal budding due to a loss of membrane integrity, as has been demonstrated in earlier studies (Aygun, 2020; Pedone, 2017). At-PtNPs can result in increasing the formation of reactive oxygen species (ROS), resulting in down-regulation of DNA, oxidative stress, and finally apoptosis of bacterial cells (Pedone, 2017). At-PtNPs exhibited considerable antibacterial activity owing to their small size, uniform dispersion, and spherical shape. Generally, nanoparticles with small particle sizes often have a higher surface area and so are more effective than those with larger particle sizes. The antibacterial activity is usually related to the local activity of the material that eliminates or reduces bacteria's growth, without general tissue toxicity (Hajipour, 2012). Various studies have shown that both the physical and chemical properties including size, shape, and surface-volume relation of nanoparticles are associated with their antibacterial activities not only the surface charge, as well as their method of synthesis (Allaker, 2010). Moreover, it was previously revealed that negatively charged AgNPs can attack the gram-negative bacteria by metal depletion as proposed by many workers (Fayaz, 2010; Amro, 2000). As a consequence, the acquired data revealed that the newly synthesized At-PtNPs constitute a potential antibacterial that has high efficacy against gram-negative bacteria with a high concentration ($2x10^8$ CFU/mL). A comparison between the antibacterial potency of At-PtNPs and other different nanoparticles is provided in Table 3.

3.9.3. Antioxidant study

The production of by-products such as perilous and noxious free radicals including reactive oxygen species (ROS) is generally related to common metabolic processes, which are deemed to be quintessential for the survival and welfare of biotic entities including humans (Sen, 2010; Mittler, 2017). These free radicals commonly result in oxidative stress and other physiological problems (Hosny and Fawzy, 2021). DPPH has been thought of as one of the most important and common free radicals that can negatively affect human cells (Patil, 2019). DPPH is identified as a stable free radical by virtue of the delocalization of the free electron over the molecule as a whole, so that it is presumed to be not easily degradable, like the preponderance of other free radicals (Kedare and Singh, 2011; Thaipong, 2006). DPPH has long been used to test the free radical scavenging capacity of antioxidants as it is an uncharged free radical that can accept hydrogen or free electrons and lead to the production of a stable diamagnetic molecule (Nakkala et al., 2016; Mensor, 2001). A substantial and efficient role against harmful free radicals including DPPH is usually played by antioxidants such as nanomaterials including metallic nanoparticles, metal oxides, graphene, and other nanostructures (Bhakya, 2016; Shah, 2017). On mixing the DPPH solution with a substance that can donate a hydrogen

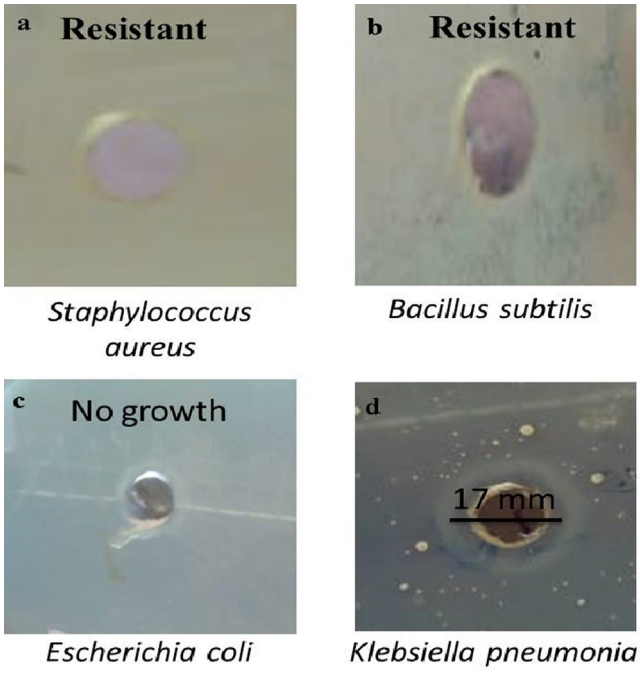

Fig. 12 Antibacterial effect of At-PtNPs against **(a)** *Staphylococcus aureus* **(b)** *Bacillus subtilis* **(c)** *Escherichia coli* **(d)** *Klebsiella pneumonia*.

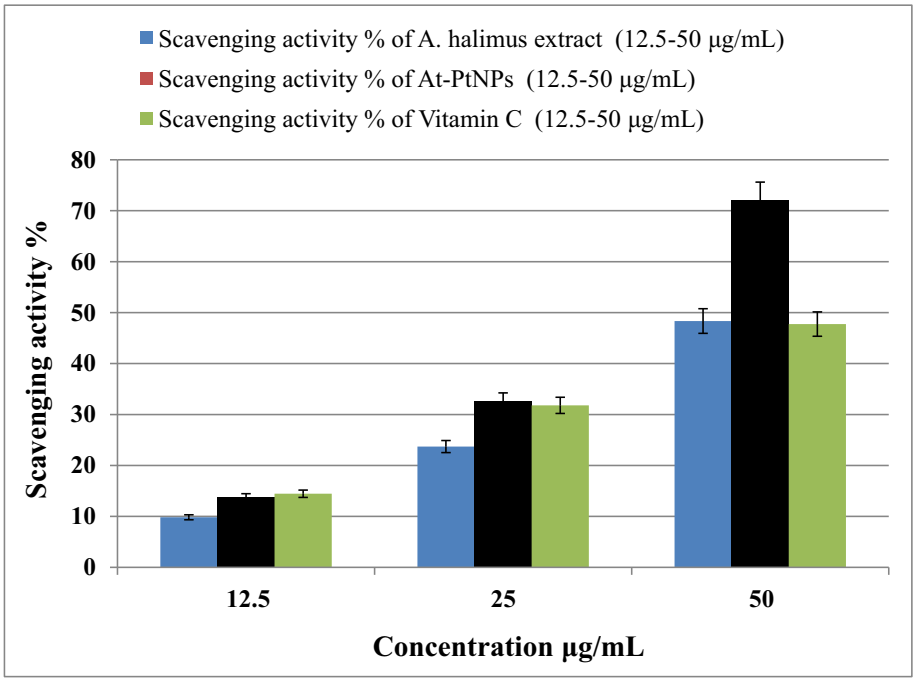

Fig. 13 Antioxidant efficiency of *A. halimus* extract, At-PtNPs, and Vitamin C (positive control) against DPPH.

atom, in other words, it is working as an antioxidant, it causes the formation of the reduced form confirmed by the loss of the characteristic violet color (Sharma and Bhat, 2009) such as gold, palladium, silver, platinum, and other metallic nanoparticles which commonly play an essential role in eliminating DPPH (Zayed, 2020; Lee, 2014; Singh and Dhaliwal, 2019). In the current study, the scavenging % of DPPH increased dramatically from 13.77% to approximately 72% when the concentration of At-PtNPs increased from 12.5 to 50 µg/mL as shown in Fig. 13 which is reckoned to be a promising and a high percentage compared to most of the scavenging percentages mentioned by other studies (Selvi, 2020; Ramachandiran et al., 2021) that could be attributed to the biomolecules of *A. halimus* extract that led to the formation of highly stable and efficient PtNPs. In addition, the IC50 was figured out to be 36 µg/mL confirming the high antioxidant efficiency of At-PtNPs. Concerning the efficacy of *A. halimus* extract, it improved from 9.83% to 48.35% when the concentration of this extract increased in the same manner as At-PtNPs. Vitamin C, which was used as a positive control, achieved 14.45%, 31.8%, and 47.75% of DPPH scavenging at the concentrations of 12.5, 25, and 50 µg/mL (Fig. 13), in a respective manner, which is lower than At-PtNPs. Therefore, the obtained results confirmed the high antioxidant capacity of both *A. halimus* extract and At-PtNPs against DPPH and their promising application in the scavenging of other free radicals in further work. A comparison among At-PtNPs and other metallic nanoparticles in the scavenging efficiency of DPPH is presented in Table 4.

4. Conclusion

The current work is the first to demonstrate a rapid, one-step, cost-effective, and environmentally friendly production of platinum nanoparticles (At-PtNPs) utilizing the aqueous extract of *A. halimus* leaves. The phytosynthesis of At-PtNPs using the investigated species' aqueous extract was deemed to be successful and efficient, as they were found stable for more than three months and evidenced by the formation of dark brown and spherical At-PtNPs with a zeta potential of – 25.4 mV, very fine microscopic diameter ranging between 1 and 3 nm, and a surface plasmon peak at 295 nm. At-PtNPs were confirmed to be an excellent catalyst since they were able to catalytically degrade MB at three different concentrations in no time, and at 100 ppm it took only 5 min. Against gram-negative bacteria, At-PtNPs had strong antibacterial effect as they were able to stop *Klebsiella pneumonia* from growing with an inhibition zone of 17 mm and prevent the growth of *Escherichia coli* at all. Moreover, they have been confirmed to be a highly effective antioxidant agent with an IC50 value of 36 µg/mL. So, the current findings show that using an aqueous extract of *A. halimus* to synthesize PtNPs is a straightforward and effective way for producing a powerful nanomaterial that could be efficiently employed in a variety of different applications. Additionally, it can be concluded that At-PtNPs synthesis in the current study upholds many of the principles of green chemistry such as less hazardous chemical syntheses, safer solvents and auxiliaries, design for energy efficiency, and use of renewable feedstocks.

Table 3 Comparison between the antimicrobial efficiency of At-PtNPs synthesized in the current study and other nanomaterials mentioned in other studies.

Sample	Concentration ($mg.mL^{-1}$)	Bacterial strain	Zone of inhibition (mm)	Ref.
AgNPs		Escherichia *coli*	18.5	(Hernández-Morales, 2019)
	0.0075	*Staphylococcus aureus*	14.9	
AgNPs		Escherichia *coli*	14	
		Staphylococcus aureus	13	
	–	*Pseudomonas aeruginosa*	16	(Naaz, 2021)
AuNPs	10	*Staphylococcus aureus*	24	
		Pseudomonas aeruginosa	27.5	(Bindhu and Umadevi, 2014)
AuNPs	100	*Escherichia coli*	17.6	(Bakur, 2019)
		Staphylococcus aureus	17	
AuNPs		*Bacillus subtilis*	9	
		Staphylococcus aureus	12	
		Escherichia coli	7	
		Pseudomonas aeruginosa	5	
AgNPs		*Bacillus subtilis*	10	
		Staphylococcus aureus	14	
	–	*Escherichia coli*	8	(Poojary et al., 2016)
		Pseudomonas aeruginosa	6	
		Escherichia coli	2	
PtNPs	0.5	*Staphylococcus aureus*	25	(Aygun, 2020)
		Pseudomonas aeruginosa	25	
		Pseudomonas aeruginosa	15	
PtNPs	–	*Bacillus subtilis*	18	(Tahir, 2017)
		Staphylococcus aureus	10	
		Pseudomonas aeruginosa	11	
PtNPs		*Bacillus subtilis*	Resistant	
	–	*Klebsiella pneumonia*	12	(Nishanthi et al., 2019)
At-PtNPs	1	*Escherichia coli*	No growth (sensitive)	
		Klebsiella pneumonia	17	This study
		Bacillus subtilis	Resistant	
		Staphylococcus aureus	Resistant	

Table 4 Comparison between the antioxidant efficiency of At-PtNPs synthesized in the current study and other metal nanoparticles prepared in other studies.

Antioxidant	Concentration µg/mL	Scavenging activity	Ref.
PdNPs	25	82.27	(Anju et al., 2020)
PtNPs	25	78.14	
PtNPs	1000	59.37	(Selvi, 2020)
PtNPs	100	70	(Ramachandiran et al., 2021)
AgNPs	50	89.5	(Sivasankar, 2018)
AgNPs	4	80	(Sreelekha, 2021)
AgNPs	250	85.9	(Kharat and Mendhulkar, 2016)
AgNPs	500	62	(Niraimathi, 2013)
AuNPs	300	57.70	(Hosny and Fawzy, 2021)
AuNPs	120	84.64	(Veena, 2019)
AuNPs	300	70	(Manivasagan, 2015)
AuNPs	125	50	(Bakur, 2019)
At-PtNPs	50	72	This study

Declaration of Competing Interest

The authors declare that they have no known competing financial interests or personal relationships that could have appeared to influence the work reported in this paper.

Acknowledgement

This work was financially supported by SMARTWATIR, ERANETMED-3-227 project, Academy of Scientific Research and Technology & Young Scientist Research Grant 2020, MAB Committee - Egyptian National Commission to UNESCO.

References

Abdelfatah, A.M. et al, 2021. *Green Synthesis of Nano-Zero-Valent Iron Using Ricinus Communis Seeds Extract: Characterization and Application in the Treatment of Methylene Blue-Polluted Water*. ACS. Omega.

Allaker, R.P., 2010. The use of nanoparticles to control oral biofilm formation. J. Dent. Res. 89 (11), 1175–1186.

Allen, H.K. et al, 2010. Call of the wild: antibiotic resistance genes in natural environments. Nat. Rev. Microbiol. 8 (4), 251–259.
Al-Radadi, N.S., 2019. Green synthesis of platinum nanoparticles using Saudi's Dates extract and their usage on the cancer cell treatment. Arabian J. Chem. 12 (3), 330–349.
Amro, N.A. et al, 2000. High-resolution atomic force microscopy studies of the Escherichia coli outer membrane: structural basis for permeability. Langmuir 16 (6), 2789–2796.
Anand, K. et al, 2016. Biosynthesis of palladium nanoparticles by using Moringa oleifera flower extract and their catalytic and biological properties. J. Photochem. Photobiol., B 165, 87–95.
Anju, A., Gupta, K., Chundawat, T.S., 2020. In Vitro Antimicrobial and Antioxidant Activity of Biogenically Synthesized Palladium and Platinum Nanoparticles Using Botryococcus braunii. Turkish Journal of Pharmaceutical Sciences 17 (3), 299.
Arul, V. et al, 2021. Efficient green synthesis of N, B co-doped bright fluorescent carbon nanodots and their electrocatalytic and bio-imaging applications. Diam. Relat. Mater. 116, 108437.
Arul, V., Chandrasekaran, P., Sethuraman, M., 2020. Reduction of Congo red using nitrogen doped fluorescent carbon nanodots obtained from sprout extract of Borassus flabellifer. Chem. Phys. Lett. 754, 137646.
Atta, A.M. et al, 2020. Methylene blue catalytic degradation using silver and magnetite nanoparticles functionalized with a poly (ionic liquid) based on quaternized dialkylethanolamine with 2-acrylamido-2-methylpropane sulfonate-co-vinylpyrrolidone. ACS Omega 5 (6), 2829–2842.
Aygun, A. et al, 2020. Biogenic platinum nanoparticles using black cumin seed and their potential usage as antimicrobial and anticancer agent. J. Pharm. Biomed. Anal. 179, 112961.
Bakur, A. et al, 2019. Synthesis of gold nanoparticles derived from mannosylerythritol lipid and evaluation of their bioactivities. Amb Express 9 (1), 62.
Barua, S., Mitragotri, S., 2014. Challenges associated with penetration of nanoparticles across cell and tissue barriers: A review of current status and future prospects. Nano Today 9 (2), 223–243.
Bathula, C. et al, 2020. Ultrasonically driven green synthesis of palladium nanoparticles by Coleus amboinicus for catalytic reduction and Suzuki-Miyaura reaction. Colloids Surf., B 192, 111026.
Benaissi, K. et al, 2010. Synthesis of platinum nanoparticles using cellulosic reducing agents. Green Chem. 12 (2), 220–222.
Benhammou, N., Bekkara, F.A., Panovska, T.K., 2009. Antioxidant activity of methanolic extracts and some bioactive compounds of Atriplex halimus. C. R. Chim. 12 (12), 1259–1266.
Bhakya, S. et al, 2016. Biogenic synthesis of silver nanoparticles and their antioxidant and antibacterial activity. Applied Nanoscience 6 (5), 755–766.
Bharati, S.S. et al, 2018. *Femtosecond laser fabricated Ag@ Au and Cu@ Au alloy nanoparticles for surface enhanced Raman spectroscopy based trace explosives detection*. Front. Physics 6, 28.
Bindhu, M., Umadevi, M., 2014. Antibacterial activities of green synthesized gold nanoparticles. Mater. Lett. 120, 122–125.
Bogireddy, N.K.R., Anand, K.K.H., Mandal, B.K., 2015. Gold nanoparticles—synthesis by Sterculia acuminata extract and its catalytic efficiency in alleviating different organic dyes. J. Mol. Liq. 211, 868–875.
Bonnia, N. et al, 2016. Green biosynthesis of silver nanoparticles using 'Polygonum Hydropiper'and study its catalytic degradation of methylene blue. Procedia Chem. 19, 594–602.
Brewer, M., 2011. Natural antioxidants: sources, compounds, mechanisms of action, and potential applications. Compr. Rev. Food Sci. Food Saf. 10 (4), 221–247.
Carezzano, M.E. et al, 2017. Inhibitory effect of Thymus vulgaris and Origanum vulgare essential oils on virulence factors of phytopathogenic Pseudomonas syringae strains. Plant Biology 19 (4), 599–607.
Celebioglu, A. et al, 2017. Surface Decoration of Pt Nanoparticles via ALD with TiO 2 Protective Layer on Polymeric Nanofibers as Flexible and Reusable Heterogeneous Nanocatalysts. Sci. Rep. 7 (1), 1–10.
Chandrasekaran, P., Arul, V., Sethuraman, M.G., 2020. Ecofriendly synthesis of fluorescent nitrogen-doped carbon dots from coccinia grandis and its efficient catalytic application in the reduction of methyl orange. Journal of fluorescence 30 (1), 103–112.
Chen, J. et al, 2021. Green synthesis, characterization, cytotoxicity, antioxidant, and anti-human ovarian cancer activities of Curcumae kwangsiensis leaf aqueous extract green-synthesized gold nanoparticles. Arabian J. Chem. 14, (3) 103000.
Cui, T. et al, 2021. "Stealth" dendrimers with encapsulation of indocyanine green for photothermal and photodynamic therapy of cancer. Int. J. Pharm. 600, 120502.
Dobrucka, R., 2019. Biofabrication of platinum nanoparticles using Fumariae herba extract and their catalytic properties. Saudi Journal of Biological Sciences 26 (1), 31–37.
Dong, L. et al, 2021. Green synthesis of platinum nanoclusters using lentinan for sensitively colorimetric detection of glucose. Int. J. Biol. Macromol. 172, 289–298.
Duan, H., Wang, D., Li, Y., 2015. Green chemistry for nanoparticle synthesis. Chem. Soc. Rev. 44 (16), 5778–5792.
Edison, T.N.J.I. et al, 2016. Caulerpa racemosa: a marine green alga for eco-friendly synthesis of silver nanoparticles and its catalytic degradation of methylene blue. Bioprocess Biosyst. Eng. 39 (9), 1401–1408.
El-Borady, O.M. et al, 2020. Green synthesis of gold nanoparticles using Parsley leaves extract and their applications as an alternative catalytic, antioxidant, anticancer, and antibacterial agents. Adv. Powder Technol. 31 (10), 4390–4400.
El-Borady, O.M., Fawzy, M., Hosny, M., 2021. Antioxidant, anticancer and enhanced photocatalytic potentials of gold nanoparticles biosynthesized by common reed leaf extract. Applied Nanoscience, 1–12.
El-Monaem, E.M.A. et al, 2021. Cobalt Nanoparticles Supported on Reduced Amine-Functionalized Graphene Oxide for Catalytic Reduction of Nitroanilines and Organic Dyes. NANO 16 (04), 2150039.
El-Subruiti, G., Eltaweil, A., Sallam, S., 2019. Synthesis of active MFe2O4/γ-Fe2O3 nanocomposites (metal= Ni or Co) for reduction of nitro-containing pollutants and methyl orange degradation. NANO 14 (10), 1950125.
Eltaweil, A.S. et al, 2020. Carboxymethyl cellulose/carboxylated graphene oxide composite microbeads for efficient adsorption of cationic methylene blue dye. Int. J. Biol. Macromol. 154, 307–318.
Eltaweil, A. et al, 2020. Mesoporous magnetic biochar composite for enhanced adsorption of malachite green dye: Characterization, adsorption kinetics, thermodynamics and isotherms. Adv. Powder Technol. 31 (3), 1253–1263.
Eltaweil, A.S. et al, 2020. Efficient removal of toxic methylene blue (MB) dye from aqueous solution using a metal-organic framework (MOF) MIL-101 (Fe): isotherms, kinetics, and thermodynamic studies. Desalin. Water Treat 189, 395–407.
Eltaweil, A.S. et al, 2021. Zero valent iron nanoparticle-loaded nanobentonite intercalated carboxymethyl chitosan for efficient removal of both anionic and cationic dyes. ACS Omega 6 (9), 6348–6360.
Eltaweil, A.S. et al, 2021. Highly efficient removal for methylene blue and Cu2+ onto UiO-66 metal–organic framework/carboxylated graphene oxide-incorporated sodium alginate beads. ACS Omega.
Fan, L. et al, 2021. Green synthesis of stable platinum nanoclusters with enhanced peroxidase-like activity for sensitive detection of glucose and glutathione. Microchem. J. 166, 106202.
Fayaz, A.M. et al, 2010. Biogenic synthesis of silver nanoparticles and their synergistic effect with antibiotics: a study against gram-positive and gram-negative bacteria. Nanomed. Nanotechnol. Biol. Med. 6 (1), 103–109.
Ganapuram, B.R. et al, 2015. Catalytic reduction of methylene blue and Congo red dyes using green synthesized gold nanoparticles

capped by salmalia malabarica gum. International Nano Letters 5 (4), 215–222.
Hajipour, M.J. et al, 2012. Antibacterial properties of nanoparticles. Trends Biotechnol. 30 (10), 499–511.
Hernández-Morales, L. et al, 2019. Study of the green synthesis of silver nanoparticles using a natural extract of dark or white Salvia hispanica L. seeds and their antibacterial application. Appl. Surf. Sci. 489, 952–961.
Hosny, M. et al, 2021. Comparative study on the potentialities of two halophytic species in the green synthesis of gold nanoparticles and their anticancer, antioxidant and catalytic efficiencies. Adv. Powder Technol. 32 (9), 3220–3233.
Hosny, M. et al, 2021. Comparative study between Phragmites australis root and rhizome extracts for mediating gold nanoparticles synthesis and their medical and environmental applications. Adv. Powder Technol.
Hosny, M., Fawzy, M., 2021. Instantaneous phytosynthesis of gold nanoparticles via Persicaria salicifolia leaf extract, and their medical applications. Adv. Powder Technol.
Hussain, S. et al, 2019. Platinum nanoparticles photo-deposited on SnO2-C composites: An active and durable electrocatalyst for the oxygen reduction reaction. Electrochim. Acta 316, 162–172.
Iyer, J.K. et al, 2018. Nanodiamonds facilitate killing of intracellular uropathogenic e. Coli in an in vitro model of urinary tract infection pathogenesis. PLoS ONE 13, (1) e0191020.
Jameel, M.S. et al, 2020. Rapid sonochemically-assisted green synthesis of highly stable and biocompatible platinum nanoparticles. Surf. Interfaces 20, 100635.
Jameel, M.S. et al, 2020. Rapid methanol-assisted amalgamation of high purity platinum nanoparticles utilizing sonochemical strategy and investigation on its catalytic activity. Surf. Interfaces 21, 100785.
Jameel, M.S., Aziz, A.A., Dheyab, M.A., 2020. Comparative analysis of platinum nanoparticles synthesized using sonochemical-assisted and conventional green methods. Nano-Structures & Nano-Objects 23, 100484.
Kedare, S.B., Singh, R., 2011. Genesis and development of DPPH method of antioxidant assay. J. Food Sci. Technol. 48 (4), 412–422.
Kharat, S.N., Mendhulkar, V.D., 2016. Synthesis, characterization and studies on antioxidant activity of silver nanoparticles using Elephantopus scaber leaf extract. Mater. Sci. Eng., C 62, 719–724.
Konishi, Y. et al, 2007. Bioreductive deposition of platinum nanoparticles on the bacterium Shewanella algae. J. Biotechnol. 128 (3), 648–653.
Kora, A.J., Rastogi, L., 2016. Catalytic degradation of anthropogenic dye pollutants using palladium nanoparticles synthesized by gum olibanum, a glucuronoarabinogalactan biopolymer. Ind. Crops Prod. 81, 1–10.
Lee, J.-W. et al, 2014. Characterization of the antioxidant activity of gold@ platinum nanoparticles. RSC Adv. 4 (38), 19824–19830.
Liu, S.-T. et al, 2014. Microwave-enhanced catalytic degradation of methylene blue by porous MFe2O4 (M = Mn, Co) nanocomposites: Pathways and mechanisms. Sep. Purif. Technol. 135, 35–41.
Mahmoud, M.A. et al, 2012. Effect of the dielectric constant of the surrounding medium and the substrate on the surface plasmon resonance spectrum and sensitivity factors of highly symmetric systems: silver nanocubes. J. Am. Chem. Soc. 134 (14), 6434–6442.
Maisa'a, W., Awwad, A.M., 2021. A novel route for the synthesis of copper oxide nanoparticles using Bougainvillea plant flowers extract and antifungal activity evaluation. Chem. Int. 7 (1), 71–78.
Mallikarjuna, K. et al, 2017. Green synthesis of palladium nanoparticles using fenugreek tea and their catalytic applications in organic reactions. Mater. Lett. 205, 138–141.
Mallikarjuna, K. et al, 2019. Au-Pd bimetallic nanoparticles embedded highly porous Fenugreek polysaccharide based micro networks for catalytic applications. Int. J. Biol. Macromol. 126, 352–358.
Manivasagan, P. et al, 2015. Extracellular synthesis of gold bionanoparticles by Nocardiopsis sp. and evaluation of its antimicrobial, antioxidant and cytotoxic activities. Bioprocess Biosyst. Eng. 38 (6), 1167–1177.
Mensor, L.L. et al, 2001. Screening of Brazilian plant extracts for antioxidant activity by the use of DPPH free radical method. Phytother. Res. 15 (2), 127–130.
Mittler, R., 2017. ROS are good. Trends Plant Sci. 22 (1), 11–19.
Muthu, K., Priya, S., 2017. Green synthesis, characterization and catalytic activity of silver nanoparticles using Cassia auriculata flower extract separated fraction. Spectrochim. Acta Part A Mol. Biomol. Spectrosc. 179, 66–72.
Naaz, R. et al, 2021. Green synthesis of silver nanoparticles using Syngonium podophyllum leaf extract and its antibacterial activity. Mater. Today:. Proc.
Nakkala, J.R., Mata, R., Sadras, S.R., 2016. The antioxidant and catalytic activities of green synthesized gold nanoparticles from Piper longum fruit extract. Process Saf. Environ. Prot. 100, 288–294.
Naseer, A. et al, 2020. Biogenic and eco-benign synthesis of platinum nanoparticles (Pt NPs) using plants aqueous extracts and biological derivatives: environmental, biological and catalytic applications. J. Mater. Res. Technol. 9 (4), 9093–9107.
Niraimathi, K. et al, 2013. Biosynthesis of silver nanoparticles using Alternanthera sessilis (Linn.) extract and their antimicrobial, antioxidant activities. Colloids Surf., B 102, 288–291.
Nishanthi, R., Malathi, S., Palani, P., 2019. Green synthesis and characterization of bioinspired silver, gold and platinum nanoparticles and evaluation of their synergistic antibacterial activity after combining with different classes of antibiotics. Mater. Sci. Eng., C 96, 693–707.
Noruzi, M., Zare, D., Davoodi, D., 2012. A rapid biosynthesis route for the preparation of gold nanoparticles by aqueous extract of cypress leaves at room temperature. Spectrochim. Acta Part A Mol. Biomol. Spectrosc. 94, 84–88.
Oh, M.-M., Carey, E.E., Rajashekar, C., 2009. Environmental stresses induce health-promoting phytochemicals in lettuce. Plant Physiol. Biochem. 47 (7), 578–583.
Omer, A.M. et al, 2021. Formulation and Antibacterial Activity Evaluation of Quaternized Aminochitosan Membrane for Wound Dressing Applications. Polymers 13 (15), 2428.
Pandey, S., Mishra, S.B., 2014. Catalytic reduction of p-nitrophenol by using platinum nanoparticles stabilised by guar gum. Carbohydr. Polym. 113, 525–531.
Patil, M.P. et al, 2019. Extracellular synthesis of gold nanoparticles using the marine bacterium Paracoccus haeundaensis BC74171T and evaluation of their antioxidant activity and antiproliferative effect on normal and cancer cell lines. Colloids Surf., B 183, 110455.
Pedone, D. et al, 2017. Platinum nanoparticles in nanobiomedicine. Chem. Soc. Rev. 46 (16), 4951–4975.
Poojary, M.M., Passamonti, P., Adhikari, A.V., 2016. Green synthesis of silver and gold nanoparticles using root bark extract of Mammea suriga: characterization, process optimization, and their antibacterial activity. BioNanoScience 6 (2), 110–120.
Rahman, S.M.A. et al, 2011. Antibacterial activity of some wild medicinal plants collected from western Mediterranean coast, Egypt: Natural alternatives for infectious disease treatment. Afr. J. Biotechnol. 10 (52), 10733–10743.
Rajeshkumar, S., 2016. Anticancer activity of eco-friendly gold nanoparticles against lung and liver cancer cells. J. Genet. Eng. Biotechnol. 14 (1), 195–202.
Ramachandiran, D., Elangovan, M., Rajesh, K., 2021. Structural, optical, biological and photocatalytic activities of platinum nanoparticles using salixtetraspeama leaf extract via hydrothermal and ultrasonic methods. Optik 167494.
Şahin, B. et al, 2018. Cytotoxic effects of platinum nanoparticles obtained from pomegranate extract by the green synthesis method on the MCF-7 cell line. Colloids Surf., B 163, 119–124.

Sallam, S., El-Subruiti, G., Eltaweil, A., 2018. Facile synthesis of Ag–γ-Fe 2 O 3 superior nanocomposite for catalytic reduction of nitroaromatic compounds and catalytic degradation of methyl orange. Catal. Lett. 148 (12), 3701–3714.

Selvi, A.M. et al, 2020. Synthesis of Tragia involucrata mediated platinum nanoparticles for comprehensive therapeutic applications: Antioxidant, antibacterial and mitochondria-associated apoptosis in HeLa cells. Process Biochem. 98, 21–33.

Sen, S. et al, 2010. Free radicals, antioxidants, diseases and phytomedicines: current status and future prospect. International journal of pharmaceutical sciences review and research 3 (1), 91–100.

Shah, R. et al, 2014. *Optimisation and stability assessment of solid lipid nanoparticles using particle size and zeta potential*. Journal of Physical. Science 25 (1).

Shah, S.T. et al, 2017. Surface functionalization of iron oxide nanoparticles with gallic acid as potential antioxidant and antimicrobial agents. Nanomaterials 7 (10), 306.

Sharma, O.P., Bhat, T.K., 2009. DPPH antioxidant assay revisited. Food Chem. 113 (4), 1202–1205.

Singh, J., Dhaliwal, A.S., 2019. Novel green synthesis and characterization of the antioxidant activity of silver nanoparticles prepared from Nepeta leucophylla root extract. Anal. Lett. 52 (2), 213–230.

Sivasankar, P. et al, 2018. Characterization, antimicrobial and antioxidant property of exopolysaccharide mediated silver nanoparticles synthesized by Streptomyces violaceus MM72. Carbohydr. Polym. 181, 752–759.

Sreelekha, E. et al, 2021. A comparative study on the synthesis, characterization, and antioxidant activity of green and chemically synthesized silver nanoparticles. BioNanoScience 11 (2), 489–496.

Subhan, F. et al, 2020. Unusual Pd nanoparticle dispersion in microenvironment for p-nitrophenol and methylene blue catalytic reduction. J. Colloid Interface Sci. 578, 37–46.

Syed, A., Ahmad, A., 2012. Extracellular biosynthesis of platinum nanoparticles using the fungus Fusarium oxysporum. Colloids Surf., B 97, 27–31.

Tahir, K. et al, 2017. Facile and green synthesis of phytochemicals capped platinum nanoparticles and in vitro their superior antibacterial activity. J. Photochem. Photobiol., B 166, 246–251.

Thaipong, K. et al, 2006. Comparison of ABTS, DPPH, FRAP, and ORAC assays for estimating antioxidant activity from guava fruit extracts. J. Food Compos. Anal. 19 (6–7), 669–675.

Thirumurugan, A. et al, 2016. Green synthesis of platinum nanoparticles using Azadirachta indica – An eco-friendly approach. Mater. Lett. 170, 175–178.

Thirumurugan, A. et al, 2016. Green synthesis of platinum nanoparticles using Azadirachta indica–An eco-friendly approach. Mater. Lett. 170, 175–178.

Ullah, S. et al, 2017. Bio-fabrication of catalytic platinum nanoparticles and their in vitro efficacy against lungs cancer cells line (A549). J. Photochem. Photobiol., B 173, 368–375.

Veena, S. et al, 2019. Green synthesis of gold nanoparticles from Vitex negundo leaf extract: characterization and in vitro evaluation of antioxidant–antibacterial activity. J. Cluster Sci. 30 (6), 1591–1597.

Walker, D. et al, 2014. Atriplex halimus L.: Its biology and uses. J. Arid Environ. 100, 111–121.

Wang, D., Lippard, S.J., 2005. Cellular processing of platinum anticancer drugs. Nat. Rev. Drug Discovery 4 (4), 307–320.

Yang, C. et al, 2017. Bio-synthesis of peppermint leaf extract polyphenols capped nano-platinum and their in-vitro cytotoxicity towards colon cancer cell lines (HCT 116). Mater. Sci. Eng., C 77, 1012–1016.

Yang, C. et al, 2018. Graphene supported platinum nanoparticles modified electrode and its enzymatic biosensing for lactic acid. J. Electrochem. Soc. 165 (14), B665.

Zada, S. et al, 2018. Biofabrication of gold nanoparticles by Lyptolyngbya JSC-1 extract as super reducing and stabilizing agents: Synthesis, characterization and antibacterial activity. Microb. Pathog. 114, 116–123.

Zayed, M.F. et al, 2020. In-vitro antioxidant and antimicrobial activities of metal nanoparticles biosynthesized using optimized Pimpinella anisum extract. Colloids Surf., A 585, 124167.

Zou, F. et al, 2018. Functionalization of silk with in-situ synthesized platinum nanoparticles. Materials 11 (10), 1929.